Avoiding Catastrophic Disassembly:
Vibrations During Rocket Launch
E80 Section 4, Team 4
May 4, 2016

Jessica Lupanow
Sean Mahre
Eyassu Shimelis
Tina Zhu

1. Abstract

In this study, the rotational and surface vibrations were studied in an effort to reduce payload vibrations and avoid catastrophic disassembly. To accomplish this, four piezoelectric sensors and an inertial measurement unit were used over the course of four flights.

The first two flights with H128 and G80 motors were used to verify the experimentally modeled antinodes and peak surface vibration frequencies below 550 Hz and create a baseline for both types of vibrations. As no sensors were placed on nodes and all but one peak were below 550 Hz, the experimental model was validated. The mathematical model suggested that by changing the density and shifting the center of mass forward, the natural frequency would go down and the stability would increase, so mass was added to the nose cone. The computational model verified this as increasing the mass of the nose cone produced a natural frequency decrease ranging from 0.0012 Hz for the first natural frequency to 0.0628 Hz for the fourth.

The third flight with a G80 motor and a mass of 22.6 g in the nose cone showed an 85.5% decrease in the peak amplitude for the rotational vibrations, a 50% decrease in the peak amplitude of the surface vibrations, and an overall reduction of the amplitudes of frequencies above 100 Hz. The fourth flight with the H238 motor and the 75.3 g mass saw an 85.4% decrease in the peak amplitude of the rotational vibrations and again the near elimination of frequencies above 100 Hz but had a 200% increase in the peak amplitude for the surface vibration.

2. Introduction

Vibrations are more than just a nuisance during flights. During a rocket launch, they can cause harm to the human body,[1] tamper with data collection by onboard circuits, and cause the rocket to tear apart during flight. Thus, understanding vibrations is paramount to passenger and rocket safety as well as optimizing data collection. By experimentally validating a vibrational model of a rocket, modifications can be made such that vibrations are reduced, thereby reducing the aforementioned chance for "catastrophic disassembly."[1] In this study, the rotational and surface vibrations of an Aerotech Arreaux model rocket were examined during launch, where "launch" for the purposes of the study is defined as the period from the ignition of the motor to apogee.

3. Rocket Design and Experimentation
3A. Scientific and/or Engineering Goals

During the rocket flights, two types of engineering measurements were acquired: vibrations along the payload section, as well as accelerometer and gyroscope readings. The goal for this data was to better understand vibrations around the payload tube during a rocket launch so that the rocket could be modified in order to reduce the vibrations experienced during launch. This information could be used to help reduced the possibility of catastrophic disassembly during rocket flight and improve data collection by limiting high frequency vibrations of the circuitry. The goal for the first week of data was to determine the baseline vibrations experienced by the rocket during flight and use the data to verify the computational and experimental models. For the second week, a mass was added to the nose cone, shifting the center of mass forward on the rocket. This was expected to reduce the amplitude of higher frequency vibrations during the launch.

3.B Sensor Selection

Piezoelectric sensors and an inertial measurement unit were employed to effectively study the rocket's stability during flight. This combination of sensors made it possible to measure the rocket's external strains and overall motions. With the information from simulations and testing, the circuits were designed to prevent data clipping, caused by oversaturation of the sensor or data logger.

Piezoelectric sensors are paper-thin membranes that are attached to surfaces and measure strain. Due to the piezoelectric effect, the sensor creates a small voltage when strained. The sensors were wired in parallel with a high value resistor, and the voltage difference between the nodes was measured. The four sensors were placed onto the outside of the rocket's payload section: one on the nose cone and the rest on the payload tube. A tap sensor, impact hammer, and LabView VI were used to find the structural modes of the payload section. The sensors were then placed on the known anti-nodes.

The MSI FDT1-028K piezoelectric sensors used in this experiment are capable of measuring very large strains (1-2 centimeters of displacement from tip to tip). Since the rocket's exterior was fiberglassed, any deflection exceeding the sensors measurement capacity was impossible without fracturing the rocket's body. The first set of flights confirmed that the surface vibrations did not exceed the sensor's input range.

Since surface vibrations are oscillatory in nature, the sensors were designed to have a reference voltage of 1.65V, half of the maximum measurement voltage. This allows the measurements to swing about a non-zero reference voltage without being clipped. These sensors were helpful in understanding the strains occurring on very localized parts of the body tube; however, they could not be used to measure the movement of the entire body.

Inertial measurement units are electronic devices that measure acceleration and angular velocities. The IMU used in the experiment was provided and created for use in the course. It was outfitted with one high-g accelerometer, three low-g accelerometers, and two rate gyroscopes. The IMU was placed on the circuit-board, which was located in the payload section of the rocket during launch as shown in Figure 1 below. Each of the accelerometers measures acceleration in either the x, y, or z direction. Each of the gyroscopes measures angular rotation about the same axes. The additional high-g accelerometer was placed in the y direction to measure acceleration in the axis which experienced the most acceleration during launch.
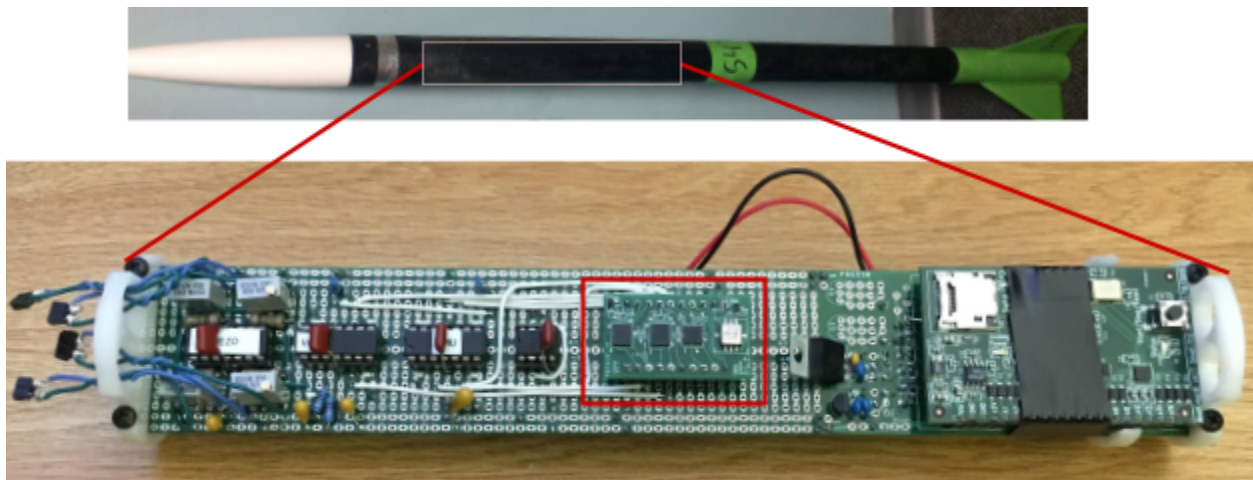

Figure 1-IMU location on circuit board and payload section.

Unlike the strain sensors placed on the body of the rocket, the IMU was used to measure translational vibrations with the accelerometer and rotational vibrations with the gyroscopes. The IMU outputs a voltage that linearly corresponded to the acceleration and angular momentum experienced as illustrated in Appendix 1 and 2.

For the motor with the largest acceleration, the H128 motor, Rocksim predicted a maximum acceleration of approximately 1397 ft/s². An IMU calibration table was used to ensure that the collected data would not be clipped at this maximum acceleration. The calibration table used a PID controlled

system to rotate a large, round table at a constant number of rotations per minute (RPM). Since rotation about a fixed point causes an acceleration in the opposite direction from the center, the table was used to apply controlled accelerative and gyroscopic motions on each axis of the IMU.

All of the signals from the sensors were passed through unity gain buffers in order to decouple the currents and resistances from the data logger.

3.C Circuit Design
3.C.1 Power Supply

The circuitry, shown in Figure 2, operated with two main voltages: 5V and 3.3V. The 5V rail powered the IMU, and the 3.3V rail supplied power to the operational amplifiers and was used to provide the virtual ground for the vibration sensors. The 5V voltage regulator is powered by the 9V battery, and the 3.3V battery is powered with the 5V output of the 7805 voltage regulator. Since it had its own internal voltage regulator, the data logger was powered directly by the 9V battery.
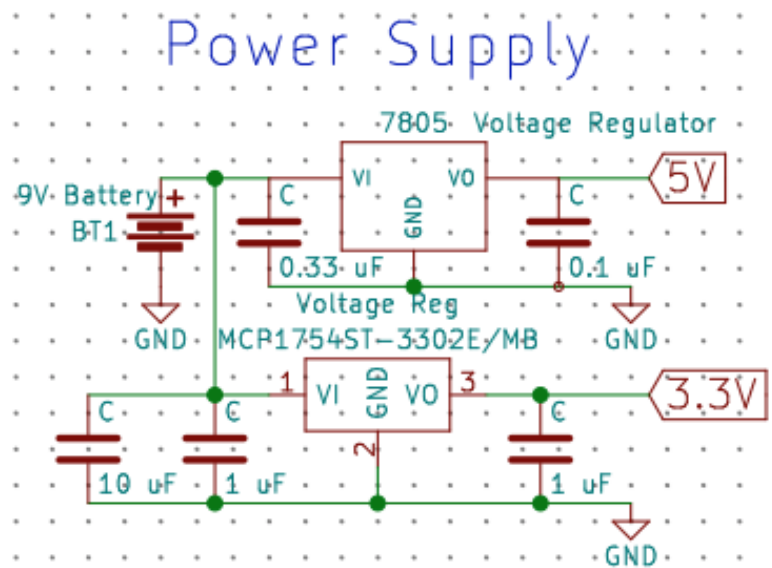

Figure 2-Power supply circuitry.

3.C.2 Piezoelectric Sensor

The piezoelectric sensors were wired in parallel with a 10MΩ resistor. When a strain is applied, the capacitance of the piezoelectric varies, which changes the voltage measured across the sensor. The output was then measured through an inverting amplifier to systematically scale the output using a potentiometer.
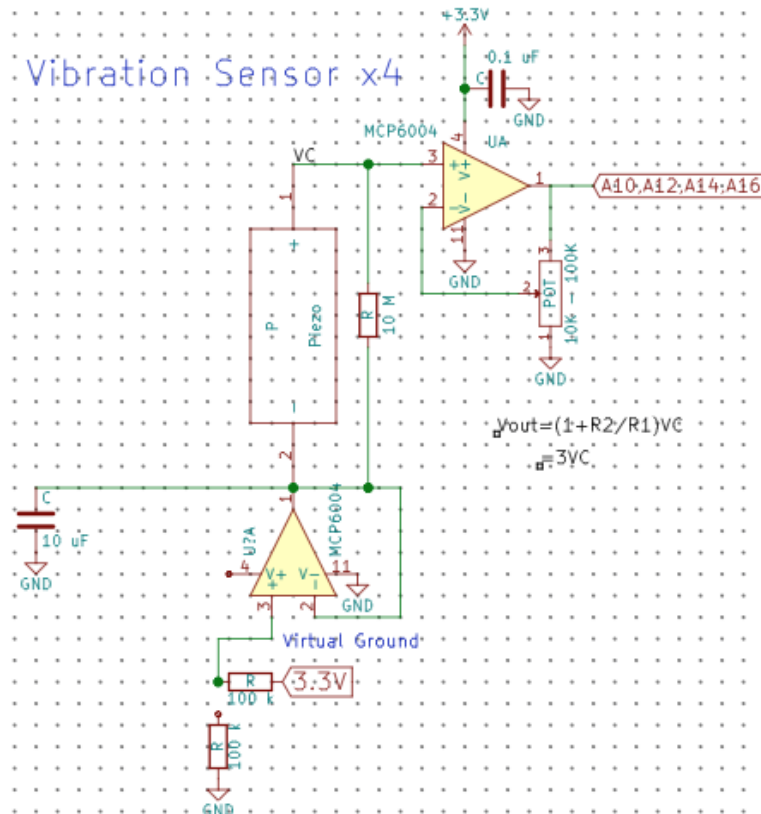
Figure 3-Vibration sensor circuitry and virtual ground.

3.C.3 Virtual Ground

In addition to the two rail voltages, the piezoelectric sensor required a midpoint reference voltage to prevent clipping. The virtual ground was created by using a voltage divider to reduce the 3.3V by half, as shown in Figure 3 above. To decouple the resistance from the rest of the sensors, the virtual ground was first supplied through a unity gain buffer.

3.C.4 IMU

All of the selected outputs, except the high-g accelerometer, were connected to the data logger through unity gain buffers as shown in Figure 4. The maximum output of the accelerometers was less than the input range of the data logger. Since the high-g accelerometer outputs a maximum of 5V, it was scaled down by two-thirds of the input value, resulting in a maximum voltage of 3.3V.
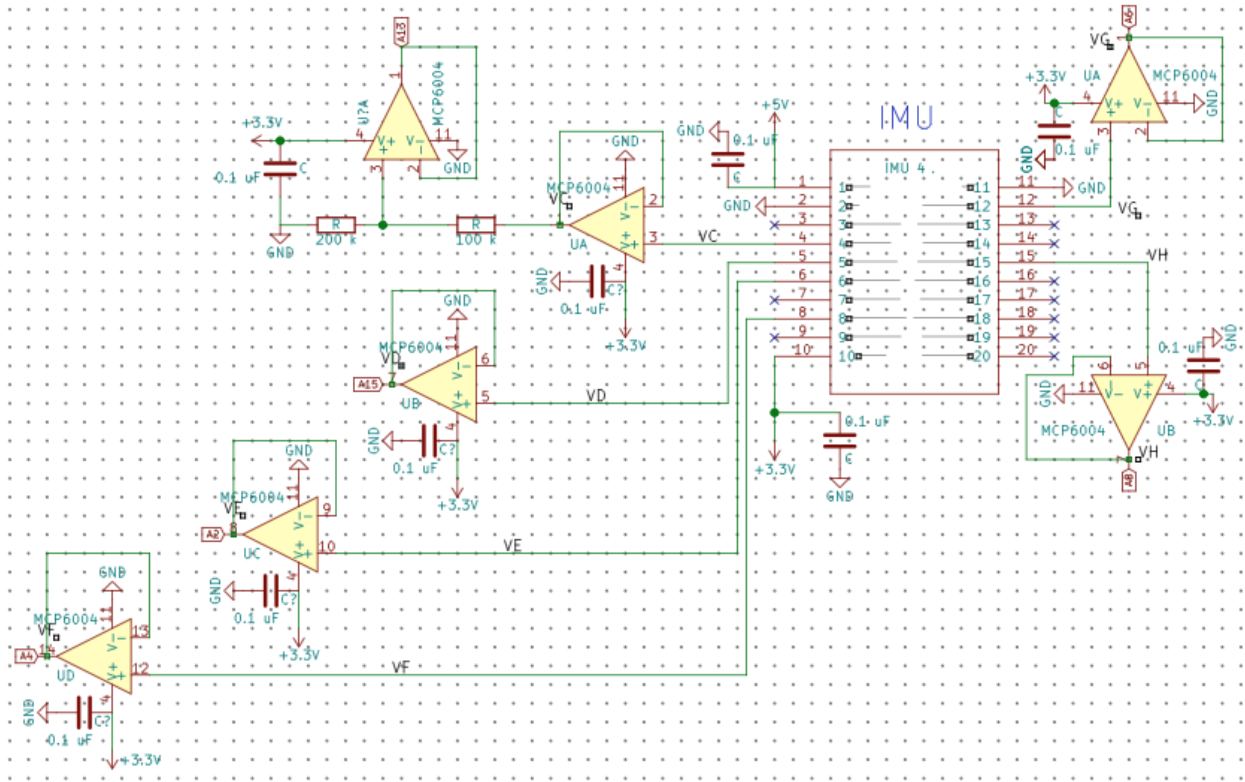
4

Figure 4-IMU Circuitry.

3.C.5 Data Logger

     The data logger, pictured below in Figure 5, was powered by the 9V battery. It was configured to sample at a rate of 64000 Hz over 12 channels, resulting in a frequency of 5333.33 Hz per channel.
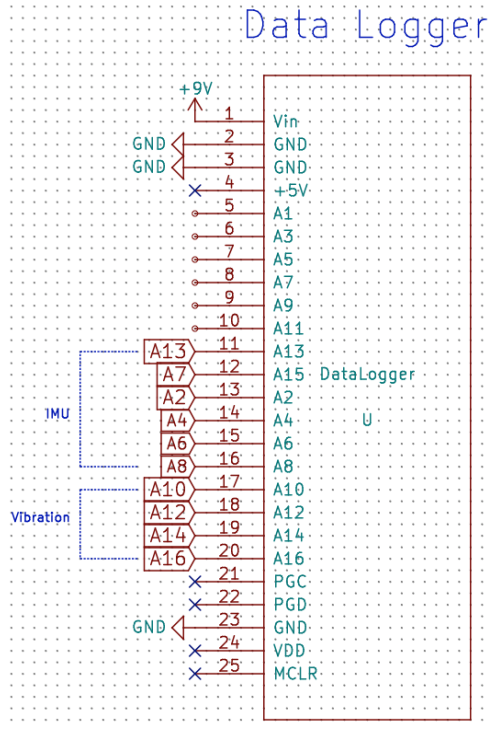
Figure 5-Data logger input.

3.D Rocket Design

The rocket used for this study was an Aerotech Arreaux. The rocket consisted of a hard plastic nose cone, a payload tube, a body tube with a motor mount, a shock cord to hold the two tubes together, and three hard plastic fins. A parachute was tied to the shock cord. The payload tube contained the PC board on which the circuits were built. The payload tube was modified from the original Arreaux design. In order to accommodate the PC board, the payload tube used in this rocket was 16.5 inches long instead of 14 inches. The components of the rocket are shown in Figures 6 and 7 below.

Figure 6-The rocket assembled.

Figure 7-The rocket disassembled.

In order to better protect the rocket, the body and payload tubes were wrapped in a fiberglass cloth. Several studies, including a study by Larry Peel, PhD at Texas A&M ,suggest that wrapping an

object in fiberglass reduces the vibrations experienced by an object.[2] This helps to stabilize the rocket during flight.

The delay charge on the G80 Motors had to be adjusted in order to eject the parachute closer to apogee. Rocksim simulations suggested that the rocket would reach apogee about 11 seconds after motor burnout, but the default delay charge was 14 seconds after motor burnout. Therefore, the delay charge was reduced to ten seconds to better match the expected flight.

The stability of a rocket as it is flying is determined in part by the position of the center of gravity relative to the center of pressure. In order for a rocket to be stable, the center of mass should be ahead of the center of pressure of the rocket. This causes lift and drag forces acting on the center of pressure to serve as restoring forces that correct any perturbations of the nose cone, thus leading to a more stable and straight flight. The further forward the center of mass is located relative to the center of pressure, the stronger the torque generated by these restoring forces will be.[3] In order to shift the center of mass of a rocket, a weight was placed in the nose cone. Two different nose cones were used in the flights. One contained a 22.6 g mass, and the other contained an 75.3 g mass. The 75.3 g mass shifted the center of mass from 28 inches from the tip of the nose cone to 25.5 inches from the tip. The 22.6 g mass shifted the center of mass to 27 inches. The weights were secured in the nose cone using a form of cyanoacrylate cement.

The vibrations sensors were placed on the outside of the nose cone and the payload tube. Vibration sensor four was placed 6 inches from the tip of the nose cone, sensor three was 12 inches from the tip, sensor one was 20 inches from the tip, and sensor two was 23 inches from the tip. A tap test analysis of the vibrational nodes of the rocket indicated that these locations would experience significant vibrations. Three holes were drilled into the payload tube of the rocket in order to allow the wires to reach the vibration sensors and the PC board.

3.E Modeling
3.E.1 Mathematical Modeling

Equation 1 describing the natural frequency of the rocket (as modeled by a single-span beam) was used to determine what could be changed to reduce the vibrational frequencies.

$$\omega_n = \beta_n^{\,2}\sqrt{EI_z/(\rho A)}$$

Equation 1-Natural frequency, ω_n, for a single-span beam where β_n is dependent on the beam's boundary conditions, E is Young's modulus, I_z is the second moment of the beam, A is the cross sectional area of the cardboard and fiberglass comprising the tube, and ρ is the density.[4]

The simplest change that could be made within the one week timeframe was an increase in the density by adding a weight to the nose cone without changing the overall volume. This would raise the center of gravity, making it even further from the center of pressure, which in turn would increase overall stability.

3.E.2 Computational Modeling

As part of the experiment, it was necessary to determine whether extra mass in the rocket nose cone would help decrease vibrations. Adding mass was expected to decrease their magnitude and frequency and would also move the center of gravity up away from the center of pressure, increasing the stability margin. To validate these expectations, Solidworks Simulation's frequency analysis study was used to model the rocket behavior., the results of which can be seen in Figures 8 and 9 for the light and heavy masses, respectively.
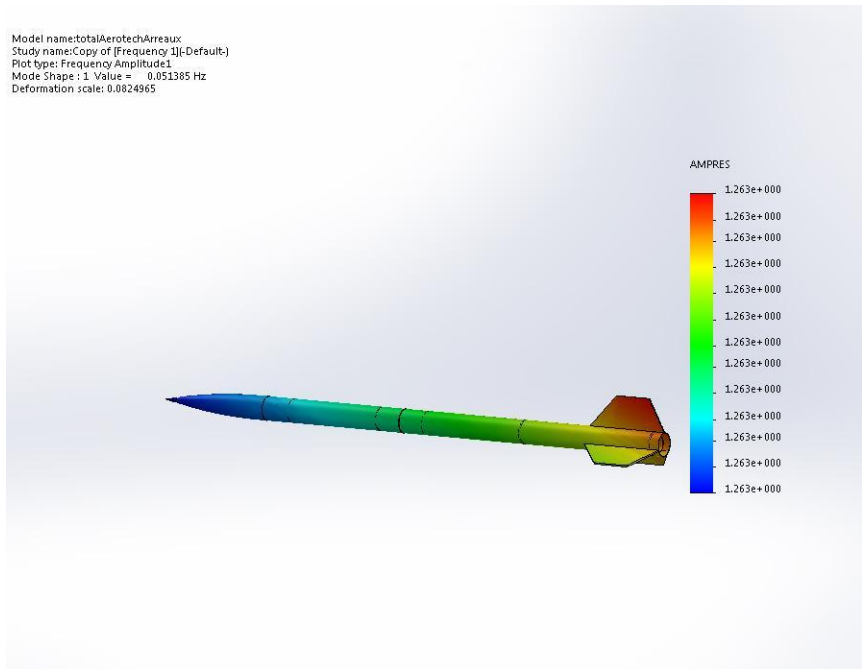
Figure 8-Simulation result for natural frequency 1 for the rocket with the light nose cone.
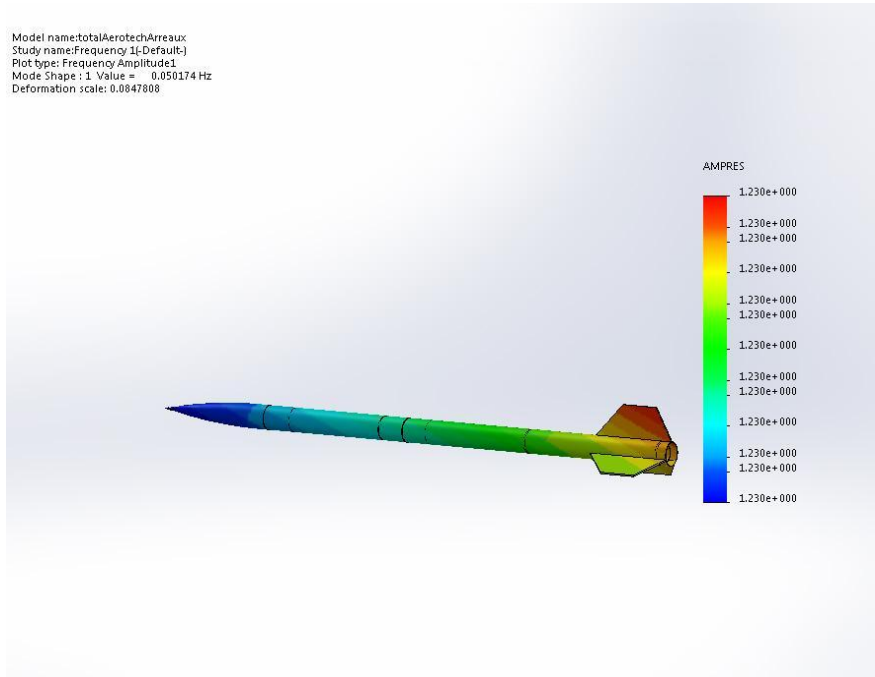

Figure 9-Sample simulation result for natural frequency 1 with the heavy nose cone.

	Heavy nose cone		Light nose cone	
Freq #	Min Ampres	Max Ampres	Min Ampres	Max Ampres

	(Normalized)	(Normalized)	(Normalized)	(Normalized)
1	1.22973 Node: 58568	1.22973 Node: 21503	1.26256 Node: 58574	1.26257 Node: 21502
2	1.22973 Node: 58575	1.22974 Node: 5101	1.26253 Node: 58575	1.26258 Node: 6360
3	1.22973 Node: 58574	1.22974 Node: 177	1.26253 Node: 58575	1.26258 Node: 5498
4	0.00240536 Node: 9801	3.00145 Node: 58575	0.00434056 Node: 15795	3.51716 Node: 58575
5	0.00151102 Node: 31852	2.99868 Node: 58575	0.00686932 Node: 18266	3.5251 Node: 58575

Table 1-Comparison of Normalized Vibration Amplitude.

Freq #	Mode List for Heavy nose cone			Mode List for Light nose cone		
	Rad/sec	Hertz	Second	Rad/sec	Hertz	Seconds
1	0.31525	0.050174	19.931	0.32286	0.051385	19.461
2	0.31546	0.050207	19.918	0.32344	0.051478	19.426
3	0.31582	0.050265	19.895	0.32354	0.051494	19.42
4	36.896	5.8723	0.17029	37.291	5.9351	0.16849
5	39.196	6.2382	0.1603	39.15	6.231	0.16049

Table 2-Comparison of Vibration Frequency with and without added mass in the nose cone.

Approximations were used in conducting the frequency analysis. The model does not have the exact material properties of the actual rocket, so some materials , such as fiberglass were approximated with plastics. The force from wind was approximated from wind velocity,[5] and was estimated to be 5 mph, or 2.2 m/s, which resulted in a 2.4 N/m^2 wind load. This was multiplied by the surface area (0.81m^2) to get the approximate force (1.94N).

Another approximation made increased the weight for the heavier nose cone by changing the nose cone material to a heavier plastic with a mass density twice that of the original rather than add a mass. Its other material properties, such as elastic modulus, are similar. In the actual rocket, however, a 3D printed mass was epoxied into the nose cone.

As shown above in Table 1, the heavier nose cone had lower maximum and minimum normalized amplitudes of vibration. Though these normalized amplitudes do not describe the actual displacement of the rocket, they do describe the relative motions of the rocket. The two studies for the heavy and light nose cones have the same scale for normalized amplitude, so the decrease in normalized amplitude shows that the heavier nose cone decreases vibrations. Table 2 also shows that the heavier nose cone has lower natural frequencies than the lighter one, ranging from a decrease of 0.0012 Hz for the first natural frequency to 0.0628 Hz for the fourth.

3.E.3 Experimental Modeling

To figure out where peaks would be in the frequency domain, a tap sensor, impact hammer, and LabView VI were used. The peaks observed are shown in Table 3.

Frequency (Hz)	550	460	250	77	77	337

Gain (dB)	15.16	28.35	18.24	20.27	13.35	32.92
Phase (rad)	3327	2135	2266	2701	2656	5143

Table 3-Results from tap test.

These peaks were put into another LabView VI to animate the vibrations of the rocket, which was used to determine the approximate locations of the nodes so the sensors could be placed nearer to the antinodes. A frame from the animation can be seen in Figure 10.
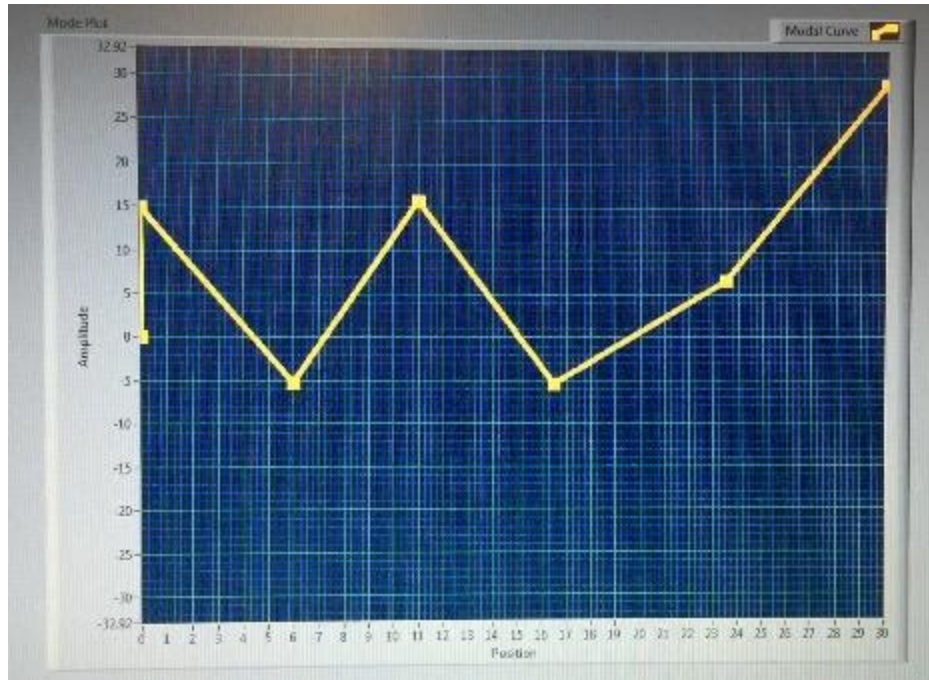

Figure 10-A still from the modal curve animation used to determine approximate locations of antinodes.

Meanwhile, the IMU was calibrated by placing the circuit board on a large rotating table. As the table rotated at a fixed number of revolutions per minute, the IMU would experience a force directly away from the center. Knowing the distance from the center to the IMU and the RPM, it was possible to calculate the force applied to the IMU as given in Equation 2.

$$a = v^2/r = ((2\pi r * RPM)/60)^2/r$$

Equation 2-Acceleration, a, where v is the linear velocity of the table, r is the radius of the table, and RPM is the number of revolutions per minute.

The gyroscopes, on the other hand, were simpler to calibrate. Since the RPM of the table was known, the angular velocity experienced is found using Equation 3.

$$\omega = RPM * (1/60) * (2\pi)$$

Equation 3-Angular acceleration on calibration table, where ω is angular velocity in rad/s.

Calibration showed that the output of the angular velocity and acceleration data was linearly related to the acceleration applied. The IMU circuit was designed to stay within range of the data logger with the information of the linear relationship and the approximated maximum values from Rocksim.

3.F Experimental Procedure

The goal for the first flight was to validate the computational model and ensure that data was collecting properly. As only the G80 motor was available both weekends, to decrease the chance of not logging data successfully on the comparable motors, the H128 was selected for the first flight. First, the flight card was filled out using the acceleration, apogee, and ejection calculations done in Rocksim. Then, the battery was tested, the data logger and sensors were tested, and the microSD card was secured with electrical tape. The second microSD card was tapped into the camera taped to the body of the rocket. The data logger was turned on, the PCB was inserted into the payload tube between pieces of foam, the vibration sensor wires were attached to the circuit, and the nose cone was secured. The parachute was loaded and the motor was prepared and inserted with the supervision of proctors. Afterward, the flight card was signed off by the RSO and LCO, and the pad number was assigned. On the pad, the rocket was loaded onto the launch rod, the camera was started, and the igniter was inserted into the motor and checked for continuity. The parachute deployed just after apogee, the rocket was recovered intact, and the data logger was turned off. The data was copied off of both microSD cards and cleared for the next flight.

The G80 motor was used for the second flight. The goal of the second flight was also to verify the computational model and provide a baseline for the vibrations without modification to be compared to the second G80 flight. The same rocket preparation occurred, but incorrect igniters were used twice before a successful launch, shock cord ripped when the parachute ejected, and the payload tube fell down unassisted. The payload was not damaged, and the rip in the shock cord was on the end near the payload tube, so the remaining shock cord was re-tied to the payload tube and an additional shock cord was tied to the payload and body tubes as well as the parachute to limit the chances of another rip. The data was again transferred to a computer for processing. Two of the sensors had come unplugged from the PCB prior to launch, so they provided no usable data.

The G80 motor was used for the third flight with a mass of 22.6 g epoxied into the nose cone. The goal of the third flight was to see if and to what degree the addition of the mass aided in reducing vibrations on the payload tube. The same preparation procedure was followed as was used in the first flight. The parachute deployed immediately at apogee, and the rocket was undamaged. The data was moved from each of the microSD cards onto the computer.

The H238 motor was used for the fourth flight with a mass of 75.3 g epoxied into a second nose cone. The goal of this final flight was to see if adding a mass to an H motor would reduce vibration. This flight could not be used to see to what degree the vibrations were reduced as the expected average thrust was nearly twice that of the previous H motor. The rocket was prepared according to the same procedure as the other flights except the motor was built at the site. The parachute ejected just after apogee, and the data was copied off each microSD card onto the computer for data analysis.

3.E Data Analysis
3.E.1 IMU (Rotational Vibrations)

The gyroscopic data was processed using Fourier analysis to examine the rotational vibrations the rocket experienced during launch. Of the three directions of rotation, only pitch and yaw were examined. The roll component was not analyzed because it is a function of the fin angles while the pitch and yaw rotations occur about the rocket's center of mass. For the purposes of measuring the angular velocity of the rocket, the distance between the center of mass and the gyroscopes did not matter because the angular displacement is the same anywhere on the axes of measurement. After collecting the data, the

accelerometers were used to find the launch time. The gyroscopic data was then processed in MATLAB to compare the magnitude of frequencies across each of the flights.

With the provided MATLAB code, the accelerometer data was plotted and used to find the time of launch. The gyroscope vibrations were then evaluated from this point until apogee.

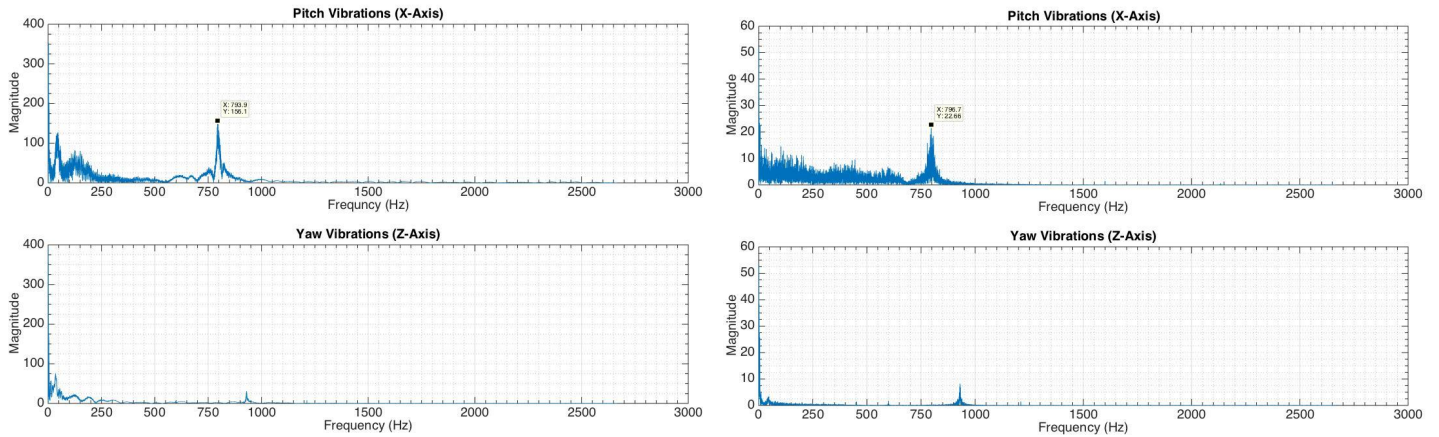G80 Motor - No Mass   G80 Motor - Light Mass

Figure 11-On the left is the second flight with G80 motor; on the right is the third flight with the light mass added to the nose cone and the same motor.

H128 Motor - No Mass   H238 Motor - Heavy Mass
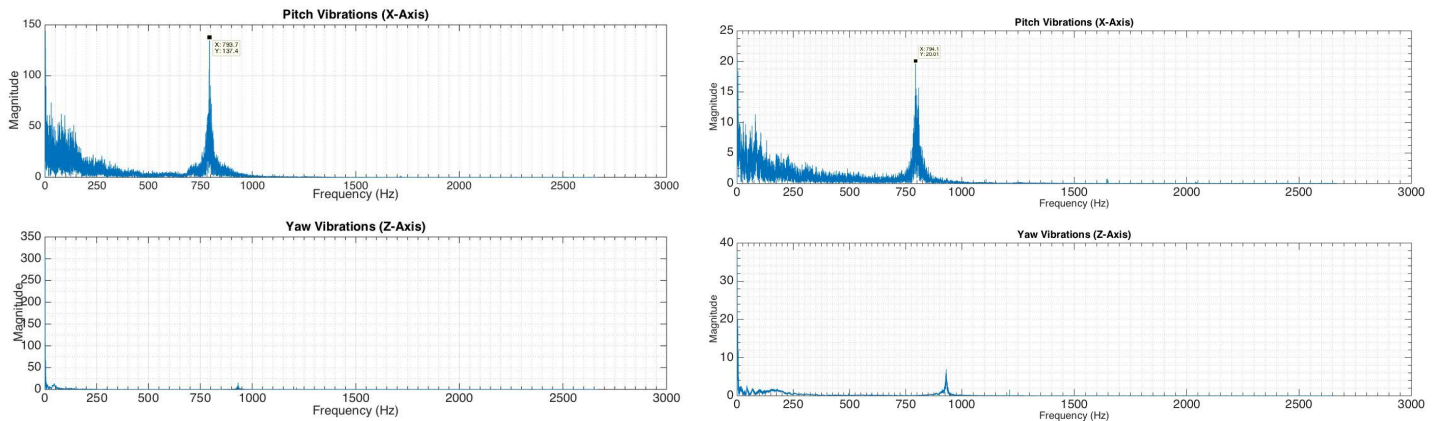
Figure 12-On the left is the first flight with H128 motor; on the right is the fourth flight with the heavy mass added to the nose cone and flying an H238 motor.

Of the four flights, only two of them had the same motors: the G80. Figure 11 above shows the effects of the nose cone mass. After adding the light mass to the nose cone, the magnitude of the 795 Hz peak dropped from 156.1 to 22.6. The other two flights used two different H motors: the H128 and the H238. The second set of comparisons is shown in Figure 12 above. The H128 had an impulse of 166 Ns,

and the H238 had an impulse of 173 Ns. The flight with the H128 had a magnitude of 137.4 at the 795 Hz peak, and the second flight with the H238 had a magnitude of 20.01 when outfitted with the heavy mass. Overall there was a 85.5% reduction in amplitude between the two G80 motors, and a 85.4% reduction in amplitude between the two H motors.

When comparing the two flights with mass (G80 and H238), there was a reduction of 11.7% when the rocket was outfitted with the heavier nose cone mass.

3.E.2 Vibration (Surface Vibration)

In order to examine the changes in surface vibration between the first two flights and the second set of flights with the added mass, the recorded voltage outputs from each sensor had to be processed. As all sensors began collecting data at the same time when the data logger was switched on, the y acceleration sensor provided an approximate time of launch. Expecting a time to apogee of 10-11 seconds, the voltage outputs of each vibration sensor from the time of launch until approximate apogee were selected as shown in Figure 13 for the first flight.
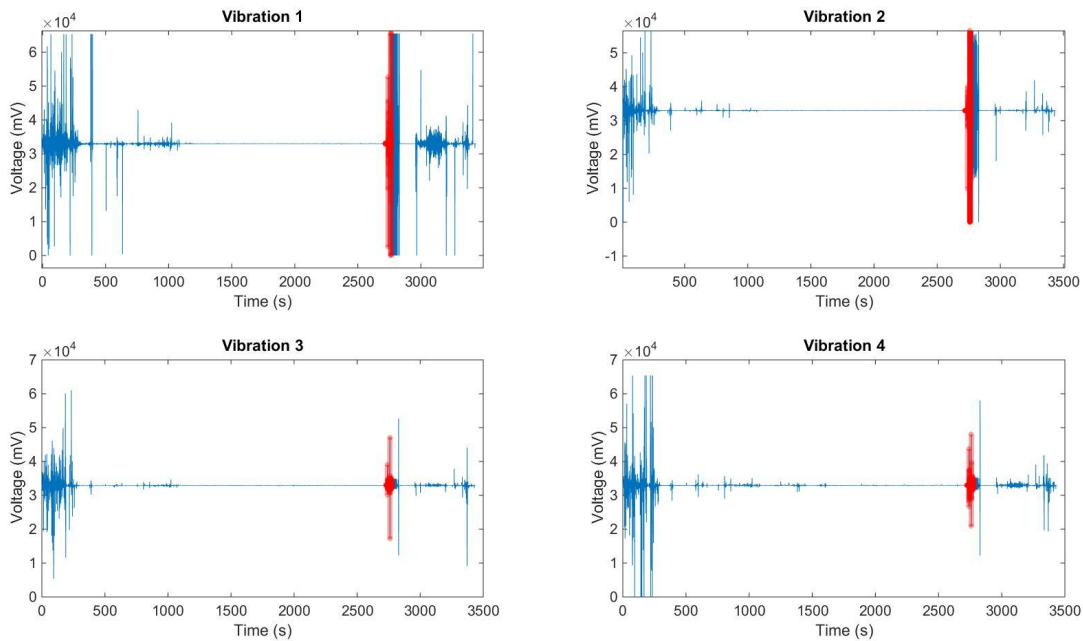

Figure 13-Selection (shown in red) of the voltage output during launch to be converted into vibration data.

Then, each selection was individually processed in MATLAB to determine the different vibrations experienced by each sensor during launch. All magnitudes are in volts as only the relative changes in vibration were considered. First, the DC offset was removed by subtracting the mean value of of the data selected and detrending. Then, the fast Fourier transform was applied to the detrended voltage data. Taking the absolute value of the result, dividing it by the number of data points, isolating the first half and multiplying by two yielded the single-sided spectrum representing the amplitudes of the frequencies experienced. Making a frequency vector that ranged from zero to the length of the vibration amplitude vector, multiplying it by the sampling frequency of 5333.33 Hz (as the data logger sampled at a rate of 64000 Hz over 12 channels), and plotting it versus the vibration vector yielded a plot of the amplitudes of the vibrations at different frequencies. Running this process for each data selection yielded the plots in Figures 14 and 15.
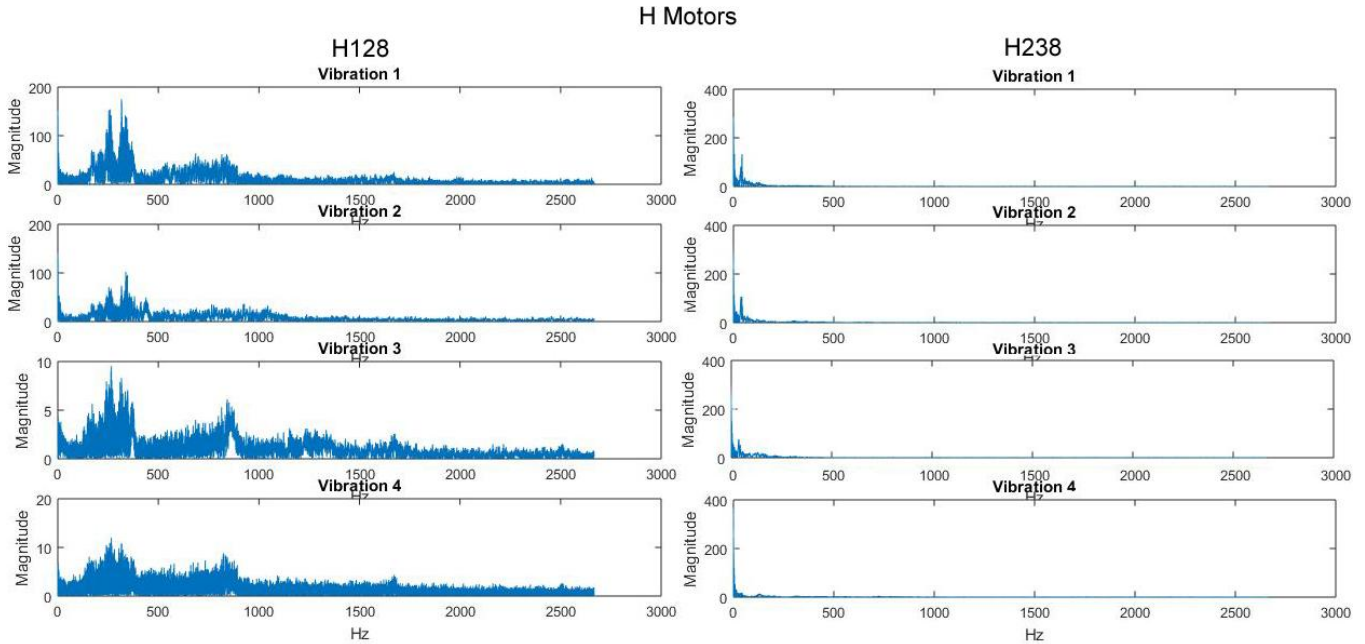
13

Figure 14-Plots depicting the amplitudes of various frequencies for the vibration experienced by each sensor during the first flight with the H128 motor and the fourth flight with the H238 motor.
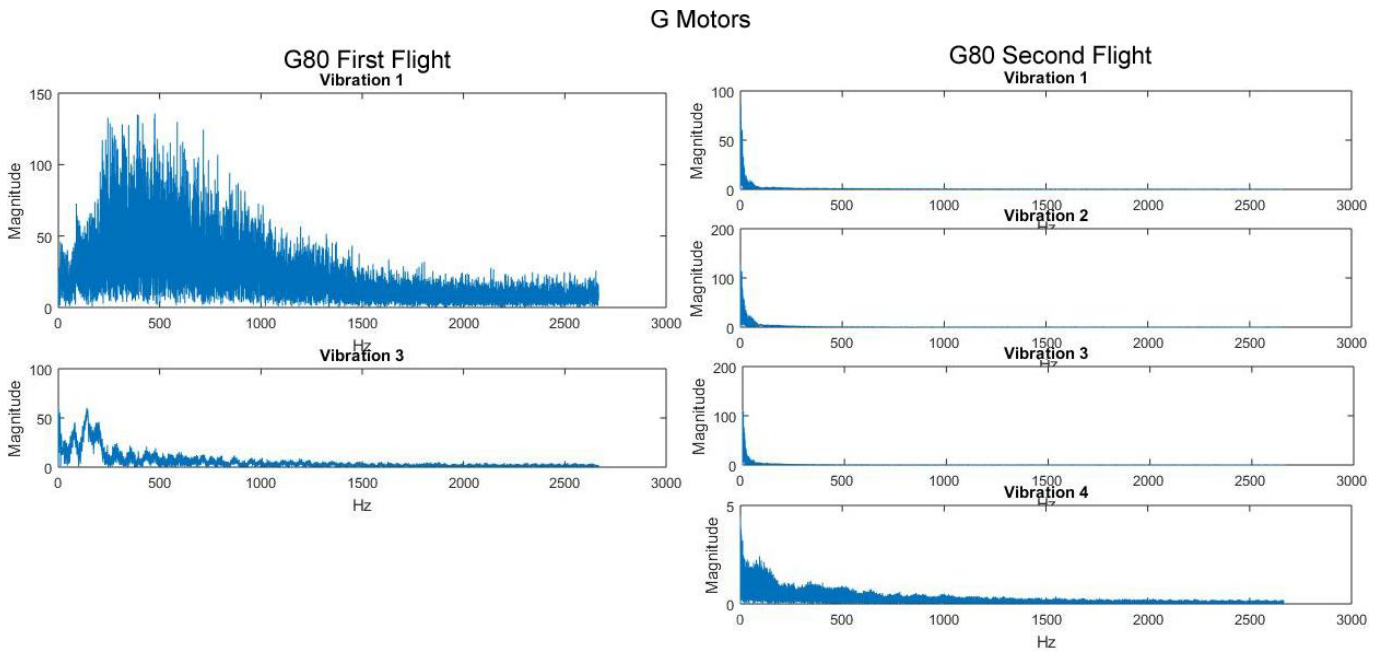

Figure 15-Plots depicting the amplitudes of various frequencies for the vibration experienced by each sensor during the second and third flights with the G80 motor.

According to Rocksim calculations prior to the flight, the H128 motor had an average thrust of 128.0 N while the H238 had an average thrust of 238.0 N. Therefore, greater vibrations were expected

from the H238's flight. Yet, by adding the weight to the nose cone for the latter flight, the amplitudes of the higher frequency vibrations (above 250 Hz) seen in sensors one and two on the payload tube in H128 flight were nearly eliminated with no noticeable increase in the amplitudes of the lower frequencies. As for the G80 motors, two of the sensors on the first flight came unplugged prior to flight, so they could not be used for comparison purposes. Sensor one, which was on the payload tube, experienced peak vibrations during the first flight between 250 and 750 Hz near 150 in magnitude while during the second flight, the peak vibration occurred at a low frequency and was less than 100 in magnitude (a 50% decrease) and all other frequencies above approximately 100 Hz approached 0 in magnitude. Sensor three showed a higher peak (nearly double that of the earlier flight), but the amplitudes again dropped off to zero below 100 Hz. Thus, for both the G and H motors, adding weights to the nose cone nearly eliminated high frequency surface vibrations on and near the payload tube but had either a negative or negligible effect on the lower frequency surface vibrations.

3.E.3 Comparing to models

The tap test from the experimental model was used for the first set of flights to indicate where peaks were to be expected and to determine the approximate location of the nodes. The test showed that the major peaks would be at 550 Hz or below. For the H128 motor, the major peaks were primarily under 500 Hz as expected with one minor peak around 800 Hz. For the G80 motor, the major peaks occurred at or below 500 Hz as well. Additionally, all of the sensors successfully collected surface vibration data, so none of them were placed at nodes.

The computational model predicted that the rocket with the heavier nose cone would have lower maximum and minimum vibration amplitudes, and a lower set of natural frequencies. The vibration data obtained from the actual flights shows that higher frequency vibrations dropped off dramatically, and the amplitudes of other frequencies decreased. Figures 16-19 show that though all the vibration sensors showed approximately a 50% decrease in maximum vibration amplitude for the heavier nose cone, vibration decreased the most for the sensor on position 3, which was attached to the payload tube.

This degree of elimination of vibrations was unexpected, because the simulation showed only a slight decrease in natural frequency and normalized vibration amplitude.
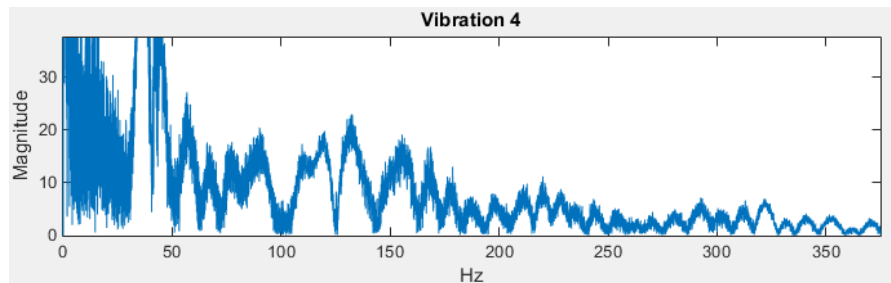

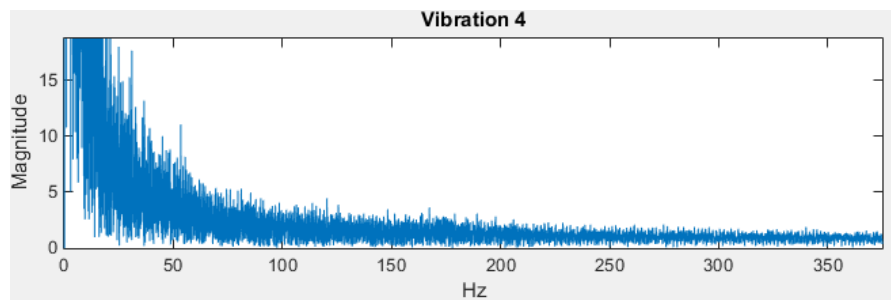Figure 16-Vibrations from sensor position 4 (on the nose cone), flight with lighter nose cone.

Figure 17-Vibrations from sensor position 4 (on the nose cone), flight with heavier nose cone.
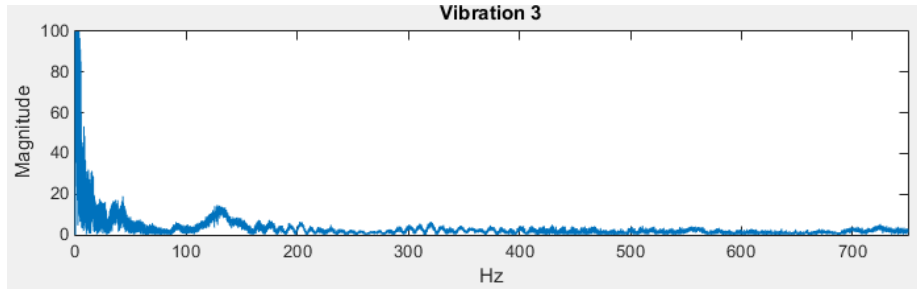

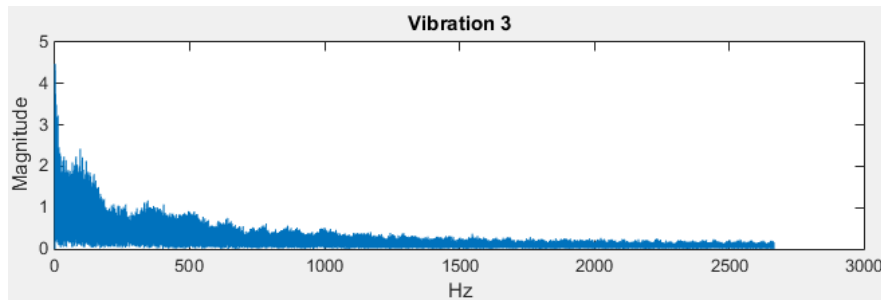Figure 18-Vibrations from sensor position 3 (on the payload tube), flight with lighter nose cone.

Figure 19-Vibrations from sensor position 3 (on the payload tube), flight with heavier nose cone.

One reason for the unexpected decrease in surface vibrations was the higher stability margin, which is not something that frequency analysis simulation (which only shows the change in natural frequencies and the change in modal shapes) could describe. A higher stability margin means that the rocket flew more into the wind than against it, which would dramatically impact lateral vibrations (while only those vibrations along the sides of the rocket were simulated).

The added mass also shifted the nodes slightly so that the vibration sensors were no longer as close to the anti-nodes; however, because modal shapes in the heavy and light nosecone Solidworks studies were similar, this is not expected to have had a large effect on the rocket vibrations.

4. Conclusion

This project validated the importance of the use of modeling in experimental engineering. Through the use of mathematical, computational, and experimental models, it was determined that adding mass to the nose cone would reduce both rotational and surface vibrations, and this was confirmed by the data collected. Though these model rockets were not very expensive or incredibly dangerous, this procedure and these types of models could be extended to larger rockets and other dynamic phenomena to reduce vibrations prior to expensive and/or potentially dangerous launches. Further analysis of the effect of density distribution and center of mass placement should be conducted to gain a deeper understanding of ways to increase safety, stability, and good data collection and avoid catastrophic disassembly.
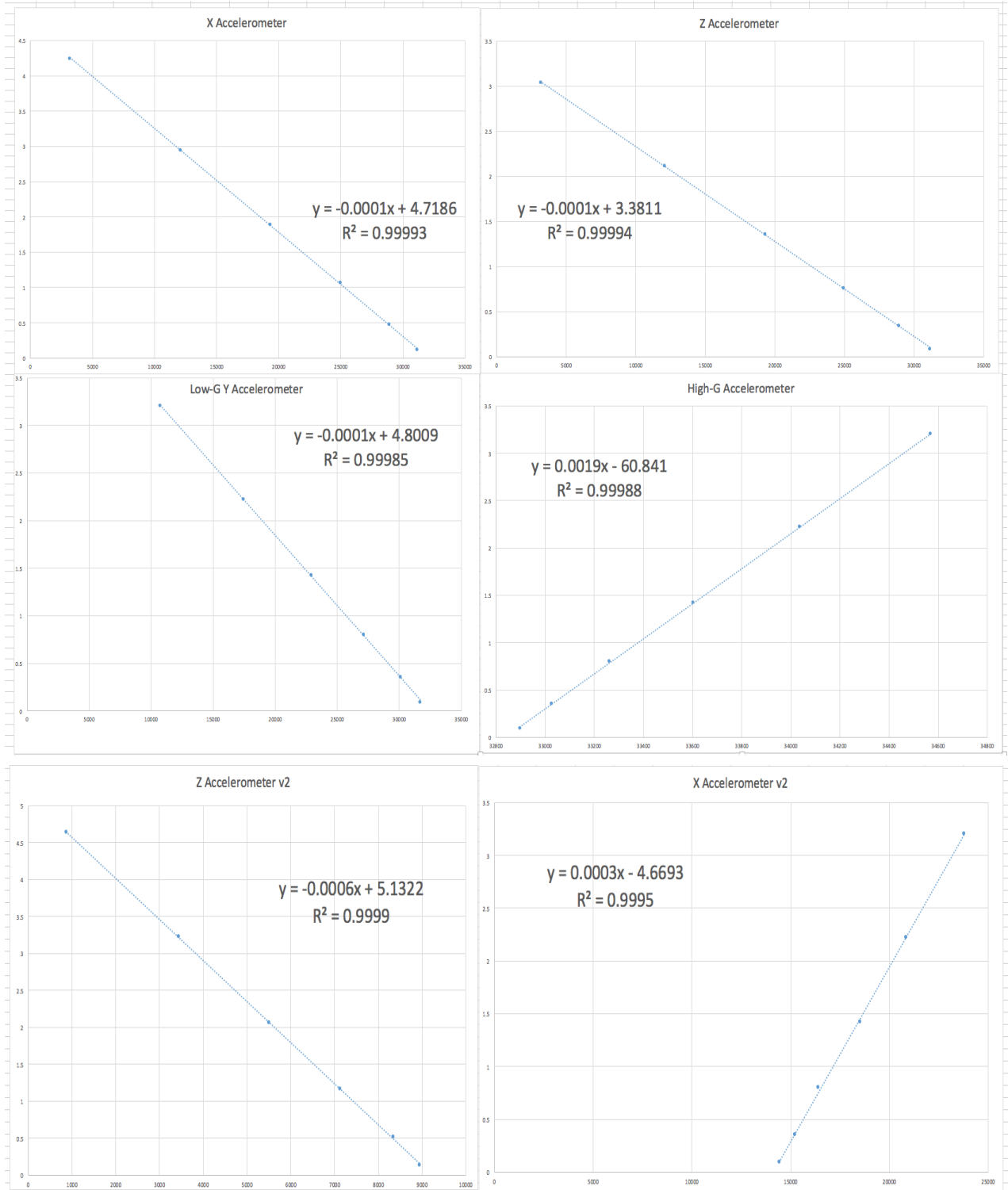
5. Acknowledgements

6. References

1). A. Lee, *Vibration and System Identification*, Harvey Mudd College Lecture (Unpublished).

2). Sharma, A., and Peel, L. (2004) , Vibration Damping of Flexible and Rigid Polyurethane Composites ,Long Beach, CA.

3). T. Benson, *Rocket Stability,* WWW Document,
 (https://spaceflightsystems.grc.nasa.gov/education/rocket/rktstab.html).

4). P. Cha, *Dynamic Beam Analytical Solution*, Harvey Mudd College Handout (Unpublished)

5).”Wind Velocity and Wind Load.” The Engineering Tool Box. N.p., 2005. Web. 3 May 2016.

Appendix
A1-Accelerometer Calibration

X Accelerometer

$y = -0.0001x + 4.7186$
$R^2 = 0.99993$

Z Accelerometer

$y = -0.0001x + 3.3811$
$R^2 = 0.99994$

Low-G Y Accelerometer

$y = -0.0001x + 4.8009$
$R^2 = 0.99985$

High-G Accelerometer

$y = 0.0019x - 60.841$
$R^2 = 0.99988$

Z Accelerometer v2

$y = -0.0006x + 5.1322$
$R^2 = 0.9999$

X Accelerometer v2

$y = 0.0003x - 4.6693$
$R^2 = 0.9995$

A2-Gyroscope Calibrations

X Gyroscope

$y = -7E-05x + 2.0266$
$R^2 = 0.9989$

Z Gyroscope

$y = -0.0003x + 8.4622$
$R^2 = 0.99873$